frontiers in Earth Science

ORIGINAL RESEARCH
published: 07 August 2020
doi: 10.3389/feart.2020.00242

Early Jurassic Rare Metal Granitic Pluton of the Central Asian Orogenic Belt in North-Central Mongolia: Tungsten Mineralization, Geochronology, Petrogenesis and Tectonic Implications

Jaroslav Dostal[1], Martin Svojtka[2], Ochir Gerel[3] and Randolph Corney[1]*

[1] Department of Geology, Saint Mary's University, Halifax, NS, Canada, [2] Institute of Geology, Czech Academy of Sciences, Prague, Czechia, [3] Mongolian University of Science and Technology, Ulaanbaatar, Mongolia

The Tukhum granitic pluton is a part of the Mesozoic composite Khentei batholith of north-central Mongolia, which belongs to the Central Asian Orogenic Belt. The shallow-seated pluton (~900 km^2) is made up of two distinct biotite granite intrusions dated at ~191 and 183 Ma and hosts a tungsten deposit associated with the younger phase. Both intrusions are composed of ferroan A2-type granites, which are fractionated and silica-rich (>71 wt.%). Their mantle-normalized plots are relatively enriched in Cs, Rb, U, and Th and depleted in Ba, Sr, Eu, Nb, and Ti. They have $\varepsilon_{Nd}(t)$ ranging from ~0 to +1 and Nd model ages ~650–900 Ma. The granites were derived by partial melting of a Neoproterozoic middle/lower crustal source of felsic/intermediate composition, followed by fractional crystallization. The younger intrusion also contains leucogranites with a trace element composition indicative of a combined crystal and fluid fractionation. The source of this younger intrusion was enriched in rare metals (W, Sn). The tungsten deposit is associated with the last stages of the evolution of the granitic magma. The origin of the pluton as well as the Khentei batholith is related to a mantle plume, which provided the heat triggering a crustal melting. The plume resulted in the eastward movement of large-scale magmatism over time, from the Tarim traps (300–275 Ma) through the large Khangai magmatic center (270–240 Ma) to the Khentei batholith (230–180 Ma) in north-central Mongolia.

Keywords: Rare metal granite, tungsten deposit, Central Asian Orogenic Belt, U-Pb zircon dating, petrogenesis, mantle plume, Mongolia, Mesozoic

OPEN ACCESS

Edited by:
J. Gregory Shellnutt, National Taiwan Normal University, Taiwan

Reviewed by:
Ali Polat, University of Windsor, Canada
Changqian Ma, China University of Geosciences (Wuhan), China

****Correspondence:***
Jaroslav Dostal
jarda.dostal@smu.ca

Specialty section:
This article was submitted to Petrology, a section of the journal Frontiers in Earth Science

Received: *13 February 2020*
Accepted: *03 June 2020*
Published: *07 August 2020*

Citation:
Dostal J, Svojtka M, Gerel O and Corney R (2020) Early Jurassic Rare Metal Granitic Pluton of the Central Asian Orogenic Belt in North-Central Mongolia: Tungsten Mineralization, Geochronology, Petrogenesis and Tectonic Implications. Front. Earth Sci. 8:242. doi: 10.3389/feart.2020.00242

INTRODUCTION

Many tin-tungsten mineralization and deposits are spatially, temporally, and genetically associated with highly differentiated granitic intrusions worldwide (e.g., Sillitoe et al., 1975; Dostal and Chatterjee, 1995; Förster et al., 1999; Baker et al., 2005; Černý et al., 2005; Romer and Kroner, 2016; Korges et al., 2017). One of the regions with such an economically important association is north-central Mongolia where mineralized granitic bodies (e.g., Yarmolyuk and Kuzmin, 2012; Syritso et al., 2018) are a part of the huge Central Asian Orogenic Belt (CAOB), which is characterized

by voluminous juvenile crust unlike most Phanerozoic orogenic belts including Caledonides and Hercynides (e.g., Jahn et al., 2000). This study focuses on the granites associated with a *W* deposit in north-central Mongolia, where the genetic relationship of the mineralization with the granites is not clear. An investigation of the petrology, geochronology, and geochemical characteristics of the granitic pluton can constrain the petrogenesis of the granitic rocks as well as the origin of the mineralization. It can also be useful for mineral exploration, particularly if it can help to distinguish between fertile and barren granites. This is an important issue as granitic intrusions of the CAOB provide large exploration targets for W-Sn mineralization. A better understanding of the geochemical characteristics and petrogenesis of the mineralized intrusions is a significant step toward developing a strategy for mineral exploration in this region. In this paper, we present whole-rock major and trace element and Nd isotopic data as well as the U-Pb zircon ages for the granitic rocks from the Tukhum pluton (TP; north-central Mongolia) and discuss their origin and tectonic settings. In addition, the paper contributes to the current discussion on the role of a mantle plume under this part of the CAOB (e.g., Donskaya et al., 2013; Yarmolyuk et al., 2013). The composite intrusion, situated about 100 km NW of Ulaanbaatar, hosts a tungsten deposit.

GEOLOGICAL SETTING

The CAOB, a large accretionary orogen bounded by the Siberian craton to the west and north and the North China and Tarim cratons to the south, stretches from the Ural Mountains to the Pacific Ocean (**Figure 1**). It consists of numerous orogenic belts (e.g., Sengör et al., 1993; Jahn et al., 2000), some of which are characterized by widespread granitoid magmatism ranging in age from the Late Precambrian to the Mesozoic. In northern Mongolia and southern Siberia, along the southern border of the Siberian craton, the CAOB contains voluminous Late Paleozoic to Mesozoic granitoid rocks including large batholiths (such as Khangai and Khentei) surrounded by Permian–Early Cretaceous rift zones (**Figure 1**). In north-central Mongolia, the CAOB features the Daurian-Khentei megadome or uplift, a northeast-trending bulge about 600 km long and 200 to 220 km wide that has been uplifting from the early Mesozoic to the Recent. The megadome contains mainly Paleozoic turbidites intruded by the Khentei batholith, the largest Late Triassic–Early Jurassic intrusion in north-central Mongolia. The batholith is composed of numerous Mesozoic plutons, which were emplaced between 230 and 180 Ma (Yarmolyuk et al., 2013; this paper). The individual plutons vary in composition from granodiorite to leucogranite with minor amounts of gabbro and diorite as well as small bodies of Li-F-rich granite occurring along the margins of the batholith. Some of the Li-F-rich granites host the W-Sn mineralization. The intrusions of the megadome show a concentrically zoned arrangement (**Figure 2**) where the Khentei batholith is in the center of the bulge and is surrounded by three rift zones: Western Transbaikalian, Kharkhorin (Karakorum), and North Gobi. The rift zones consist of horsts, grabens, and depressions containing Upper Permian to Upper Triassic clastic sedimentary rocks and bimodal volcanic suites (Yarmolyuk et al., 2002) and Mesozoic granitic plutons (e.g., Dostal et al., 2014, 2015b; Antipin et al., 2016). The age of the plutons of the rift zones range typically between 221 and 186 Ma (Yarmolyuk et al., 2002; Dostal et al., 2014).

The rift zones and adjoining marginal parts of the Khentei batholith host mineralized granites. One of such plutons in north-central Mongolia is the TP which hosts a tungsten deposit (Tsagaan Davaa). Unlike some weakly mineralized granitic bodies such as Janchivlan and Avdar (Antipin et al., 2016), which occur in the rift zones along the margins of the Khentei batholith, Early Jurassic TP is located within the batholith but along its margins (**Figure 2**). It is one of the shallow-seated granitic intrusions, which are discordant and are surrounded by contact-metamorphic aureoles. The TP intruded into slightly metamorphosed Cambrian to Ordovician sedimentary rocks (mainly sandstones). The contact metamorphic aureole around the TP is up to 1.5 to 2 km wide. Close to the pluton, the aureole contains quartz-biotite-feldspar hornfels. The pluton is elongated and exposed over an area of ∼900 km^2. The internal structure of the TP suggests a dome-shaped intrusion. Our research focused on the southeastern part of the pluton (**Figure 3**), which hosts a tungsten deposit.

An unusual structure of the Daurian-Khentei megadome is not unique in the area. A large magmatic complex with a zonal concentric structure similar to that of the Khentei batholith occurs southwest of the study area (**Figure 1**). This Permian–Early Triassic body of comparable size consists of a granitoid core surrounded by rift zones (Yarmolyuk et al., 2008, 2013; Yarmolyuk and Kuzmin, 2011, 2012). The core of the structure, the Khangai batholith (>120,000 km^2), is composed mainly of granites and granodiorites emplaced between 270 and 240 Ma (Yarmolyuk et al., 2013). It lies between the Gobi-Altai and Northern Mongolian rift zones, which are similar to those around the Khentei batholith.

PETROGRAPHY

The pluton is composed mainly of fine- to coarse-grained biotite granites (**Figure 4**) and is composed of two intrusive phases (**Figure 3**). The first phase (including dated sample WOL-12) is made up of gray and yellowish gray fine- to medium-grained porphyritic granite with feldspar phenocrysts typically 1–3 cm in size that are enclosed in a groundmass composed of K-feldspar, plagioclase, quartz, and subordinate biotite (up to ∼10%). Amphibole, Fe-Ti oxides, secondary minerals (including carbonates), and accessory minerals occur in trace amounts. Phenocrysts, which are microcline-perthite and subordinate plagioclase, account for about 25% of the volume of the rocks. This intrusive phase contains numerous xenoliths of country rocks, particularly metasedimentary rocks. The second intrusive phase (encompassing dated samples WOL-14 and WOL-15) includes dominant porphyritic coarse-grained biotite granite and subordinate leucogranite. Porphyritic biotite granite contains feldspar phenocrysts, which are also mainly microcline-perthite

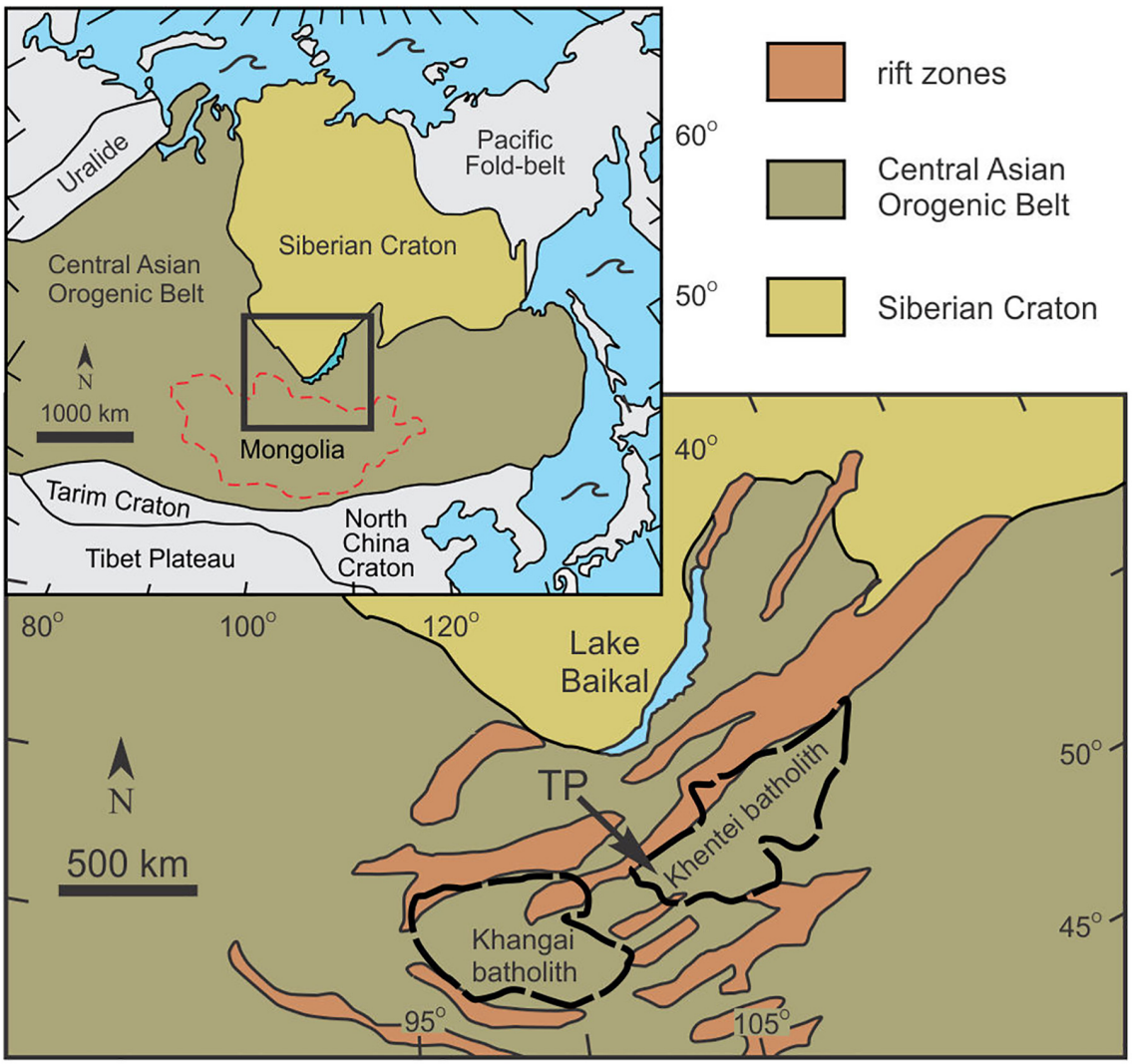

FIGURE 1 | Simplified geologic map of parts of the Central Asian Orogenic Belt and Siberian Craton showing the occurrence of two Late Paleozoic–Early Mesozoic batholiths and rift zones (modified after Yarmolyuk and Kuzmin, 2011) and the Tukham pluton (TP). Inset is a sketch map of the Central Asian Orogenic Belt, Siberian Craton, and surrounding geological provinces (modified after Jahn et al., 2009) showing the location of **Figure 1**.

and subordinate plagioclase. The groundmass is made up of plagioclase, microcline, quartz, and minor biotite and accessory minerals (titanite, zircon, Fe-Ti oxides, and pyrite). The rocks also contain minor but variable amounts of secondary minerals (chlorite, sericite, and carbonate). Compared to the rocks of the first phase, these granites have notably larger grain size. The leucogranite is composed of plagioclase (albite, albite-oligoclase), K-feldspar, quartz, secondary, and accessory minerals. These rocks mostly form bands ranging in width from a few meters to ∼100 m, which pass gradationally into the biotite granite. Some leucogranites contain dominantly primary magmatic mineral assemblages while other leucogranites, namely, those that are close to the mineralization, were affected by silicification and other alteration processes such as greisenization (quartz, dark mica, and minor fluorite). We have subdivided the altered leucogranites into moderately altered and strongly altered. Moderately altered leucogranites typically contain secondary quartz and smaller amounts of Li-bearing mica, fluorite and topaz, while the strongly altered rocks are composed mainly of a secondary mineral assemblage. It is possible that precursors of some of these strongly altered rocks were biotite granites. Porphyritic biotite granite of the second phase and leucogranite are assumed to be approximately coeval (also, e.g., Ivanova, 1976; Khasin, 1977).

TUNGSTEN MINERALIZATION

The Tsagaan Davaa tungsten deposit (Ivanova, 1976; Khasin, 1977; Jargalsaikhan, 1996) consists of wolframite-bearing quartz veins and associated greisen, which occur in the upper (apical) part (probably cupola) of the pluton. They are hosted in

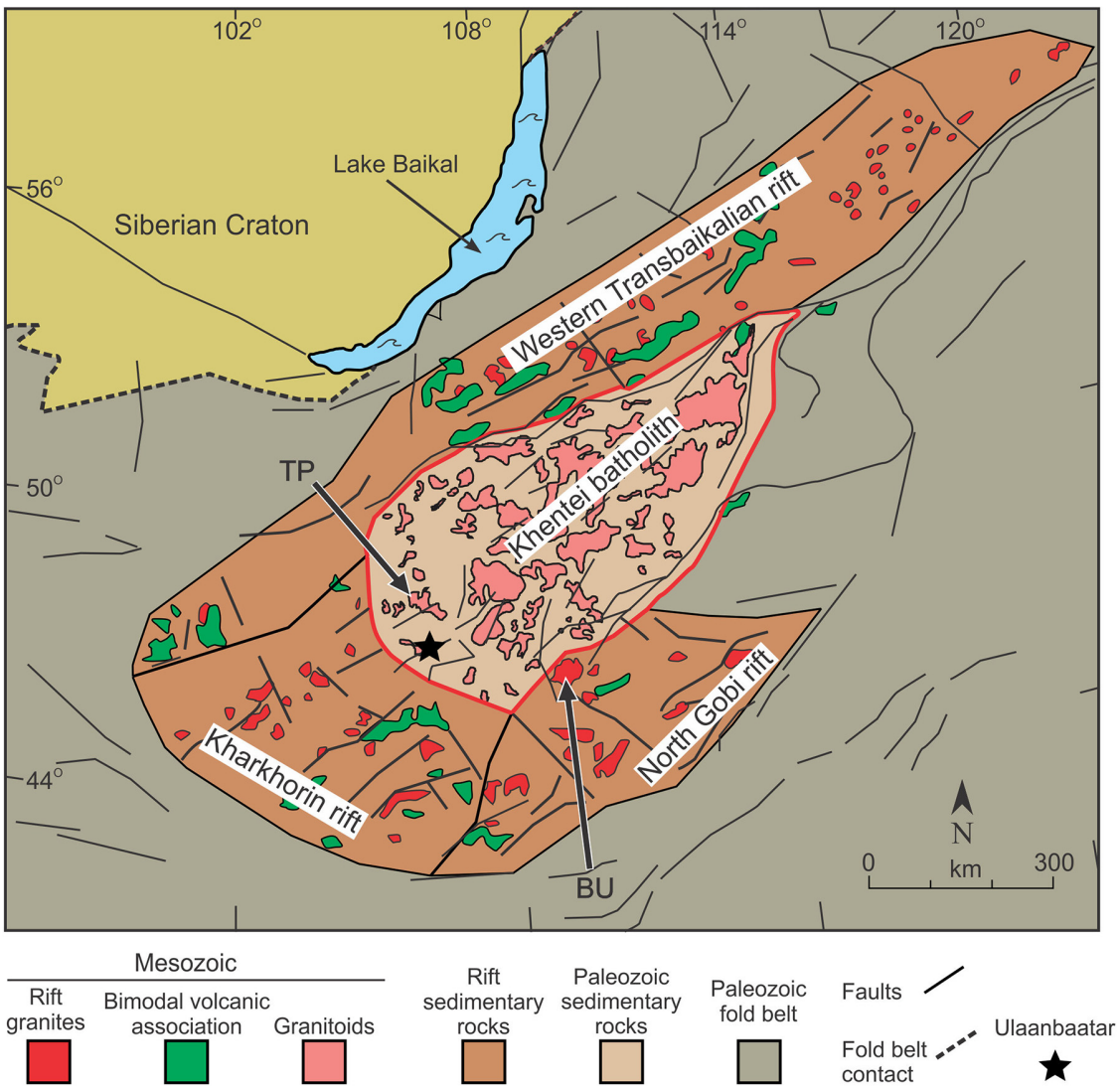

FIGURE 2 | Geologic map of the Daurian-Khentei megadome or uplift composed of the Early Mesozoic Khentei batholith, North Gobi, Kharkorin, and Western Transbaikalian rifts (modified after Yarmolyuk and Kuzmin, 2011, 2012). TP—Tukham pluton; BU—Bayan-Ulan pluton.

leucogranites, which are altered around the mineralization. Hydrothermal alteration and mineralization appear to be controlled by faults. The main mineralized zone is >1 km long and 200–500 m wide. The individual mineralized quartz veins range in thickness from <1 cm to >1 m but on an average they are ∼0.5 m thick and can be traced for tens of meters. The tungsten-bearing veins are mostly sub-horizontal bodies, gently dipping, which are parallel with the roof of the pluton and are typically accompanied by greisen and silica alteration. Greisen is the common hydrothermal alteration type associated with mineralization and is characterized by Li-F-bearing micas, fluorite, wolframite, cassiterite, and dominant quartz. The main ore mineral in the deposit is wolframite accompanied by subordinate cassiterite and molybdenite and minor scheelite, malachite, azurite, and beryl. Some veins consist almost entirely of quartz and wolframite. The deposit contained ∼3100 t of WO_3 in ore grading 1.52% WO_3 and 740 t of WO_3 in ore grading 0.72% WO_3. The grade ranges from 0.1 to 12.6% WO_3. The mine went into production in 1978.

ANALYTICAL METHODS

Whole-Rock Analyses

The analyses of whole-rock major and trace elements of the TP samples (**Table 1**) were done using lithium metaborate–tetraborate fusion at the Activation Laboratories Ltd. in Ancaster, ON, Canada. Major elements were analyzed by an inductively coupled plasma-optical emission spectrometer, whereas trace elements were determined by an inductively coupled plasma mass spectrometer (ICP-MS; Perkin Elmer Optima 3000). The accuracy for each element was monitored by analyzing

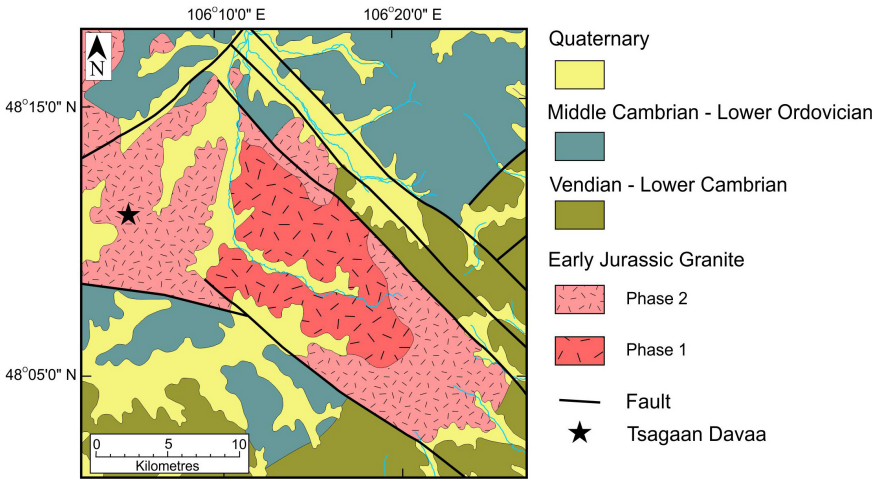

FIGURE 3 | Geological map of the southeastern part of the Tukhum pluton and surrounding units (modified after Dejidmaa, 2003; Dorjsuren and Bujinlkham, 2004) showing the location of the Tsagaan Davaa tungsten deposit.

FIGURE 4 | Photo showing a typical outcrop of the biotite granite of the Tukhum pluton (photo courtesy of Yo. Majigsuren).

international standards, which were run as unknown. Based on replicate analyses, the precision is generally better than 3% for most major elements and between 5 and 10% for trace elements. Major and some trace elements in the Bayan-Ulan samples (**Supplementary Table S2**) were determined by X-ray fluorescence at the Regional Geochemical Center at Saint Mary's University. Analytical precision as determined on replicate analyses is generally better than 5% for the major oxides and between 5% and 10% for minor and trace elements. Iron was determined as total Fe (**Table 1 Supplementary Table S2**).

Sm and Nd concentrations and Nd-isotope ratios of the granitic rocks (**Table 2**) were determined at the Atlantic Universities Regional Facility at the Department of Earth Sciences of Memorial University of Newfoundland (St. John's, Newfoundland, Canada) using a multi-collector Finnigan MAT 262 thermalionization mass spectrometer (Pollock et al., 2015). Replicate analyses of JNdi-1 yield a mean $^{143}Nd/^{144}Nd = 0.512100 \pm 6$. The 2σ values are given in **Table 2**. $\varepsilon_{Nd}(t)$ values were calculated with respect to CHUR using a present-day $^{143}Nd/^{144}Nd$ ratio of 0.512638 and a $^{147}Sm/^{144}Nd$ ratio of 0.196593, and were subsequently age-corrected. A T_{DM} model age (**Table 2**) was calculated according to the model of DePaolo (1988).

Zircon U-Pb Dating

Whole-rock samples, ca 1–2 kg in weight, were collected for mineral separation. Zircons were separated using conventional techniques: crushing, Wilfley concentration table, magnetic, and, finally, heavy liquid separations. Handpicked zircon grains were mounted in 1-inch epoxy-filled blocks, ground, and polished. Internal zircon structures were checked by cathodoluminescence (CL) imaging using scanning electron microscope at Charles University in Prague (Czech Republic). An Element 2 high-resolution sector field mass spectrometer (Thermo Scientific, Waltham, MA, United States) coupled with a 193-nm ArF Analyte Excite (Teledyne/Cetac) excimer laser ablation system at the Institute of Geology of the Czech Academy of Sciences in Prague was used to acquire the Pb/U isotopic ratios in zircons. The laser is equipped with a HelEx II active 2-volume ablation cell. The laser was fired at a repetition rate of 5 Hz, using a spot size of 25 μm. Acquisitions for standards and unknown samples consisted of a 15-s measurement of a blank followed by U and Pb signals from zircons for another 35 s. The signal was tuned for maximum sensitivity of Pb and U, Th/U ratios close to unity, and a low oxide level, commonly below 0.2%. The total of 420 mass scans data were acquired in time-resolved–peak jumping–pulse counting/analog mode with 1 point measured per peak for masses $^{204}Pb + Hg$, ^{206}Pb, ^{207}Pb, ^{208}Pb, ^{232}Th, ^{235}U, and ^{238}U. Due to a non-linear transition between the counting and analog acquisition modes of the ICP instrument and the fact that ^{238}U is usually measured in "both" mode, the raw data were preprocessed using a Python module called ExctractDat for decoding the Thermo Element ICP-MS data files (Hartman et al., 2017) and also an in-house Excel macro. As a result, the

TABLE 1 | Major and trace element compositions of granites from the Tukhum pluton.

	Phase 1			Phase 2									
Rock Type	**Granite**		**Aplite**	**Granite**				**Leucogranite**		**Altered leucogranite**		**Strongly altered granite**	
Sample	**WOL-12**	**WOL-12-1**	**WOL-13-1**	**WOL-14**	**WOL-14-1**	**WOL-15**	**WOL-15-1**	**WOL-6**	**WOL-10**	**WOL-4**	**WOL-5**	**WOL-7**	**WOL-8**
SiO_2 (wt.%)	71.99	72.86	75.07	71.86	72.96	74.36	73.71	75.27	74.79	76.86	77.08	82.47	65.85
TiO_2	0.32	0.31	0.17	0.25	0.28	0.24	0.21	0.15	0.16	0.05	0.04	0.17	0.18
Al_2O_3	13.49	13.39	12.33	13.38	13.43	12.41	13.13	12.67	12.38	12.37	12.51	7.75	18.56
$Fe_2O_3^{(t)}$	2.40	2.34	2.01	2.35	2.12	2.05	2.08	1.64	1.67	1.14	0.76	2.95	4.02
MnO	0.04	0.04	0.02	0.05	0.05	0.04	0.04	0.04	0.04	0.02	0.03	0.14	0.20
MgO	0.29	0.29	0.14	0.31	0.32	0.28	0.25	0.13	0.15	0.15	0.05	0.16	0.26
CaO	1.22	1.25	0.32	1.08	1.12	0.93	0.91	0.73	0.57	0.50	0.37	0.79	0.41
Na_2O	4.13	4.16	2.64	3.62	3.62	3.26	3.53	3.76	2.92	3.73	3.86	0.13	0.22
K_2O	4.24	4.26	6.39	4.91	4.84	4.76	5.19	4.57	5.43	4.88	4.65	2.79	6.52
P_2O_5	0.09	0.09	0.01	0.07	0.08	0.07	0.05	0.03	0.03	0.01	0.01	0.03	0.03
LOI	0.33	0.33	0.46	0.66	0.59	0.69	0.68	0.47	0.89	0.88	0.51	1.60	3.10
Σ	98.54	99.32	99.57	98.54	99.40	99.09	99.77	99.45	99.04	100.59	99.87	98.98	99.34
Sc (ppm)	2	2	1	3	3	3	3	2	2	2	2	3	7
V	10	12	8	16	21	12	12	9	6	6	2	14	20
Cu	5	5	5	5	5	10	5	150	260	460	390	590	770
Pb	27	28	37	32	33	34	34	31	32	24	39	6	13
Zn	60	60	40	50	50	50	40	140	380	710	100	590	720
Sn	2	2	3	9	9	8	6	4	27	13	4	331	374
W	0.1	0.1	0.7	3.8	2.9	2.3	2.3	2.7	9.6	3.8	3.5	12.8	53.5
Rb	155	149	181	289	293	286	293	267	471	402	303	904	1100
Cs	7.4	7.3	3.3	16.4	17.3	8.9	8.1	8.3	19.4	12.3	10.8	29.5	51.8
Ba	509	509	203	378	371	313	345	245	260	124	83	158	312
Sr	141	134	55	95	93	78	82	66	60	46	32	8	9
Ga	22	23	22	22	22	21	21	20	23	18	18	53	109
Ta	1.25	1.29	1.53	3.72	3.97	3.51	2.95	1.57	1.66	3.02	2.02	1.15	1.75
Nb	13.2	13.6	16.3	21.3	23.2	22.7	19.2	17.6	12.2	11.3	7.6	7.3	15.3
Hf	9.0	8.1	4.2	6.0	6.2	6.8	5.9	5.1	5.7	3.1	2.7	6.3	4.7
Zr	345	305	113	199	203	223	190	170	184	75	64	208	124
Y	23	24	28	51	53	38	35	53	57	59	30	68	72
Th	12.7	14.6	30.2	31.6	33.1	33.9	29.2	33.6	29.7	23.4	18.4	21.5	26.3
U	2.08	2.05	2.24	5.25	6.17	3.72	3.53	5.33	5.80	7.65	7.79	6.04	15.6
La	45.8	54.7	53.0	45.7	47.5	48.7	44.2	41.6	38.2	13.4	10.5	38.9	34.3
Ce	86.6	108	120	96.6	105	82.7	71.8	91.3	88.1	30.1	24.0	88.2	75.9
Pr	9.2	11.5	12.9	11.3	11.9	11.5	10.5	10.3	10.3	3.71	2.72	10.5	9.09
Nd	32.1	39.0	45.5	40.2	42.4	40.6	37.0	36.7	40.8	14.2	9.88	37.9	34.3
Sm	5.64	6.32	8.38	9.12	9.44	8.32	7.58	8.23	8.99	4.23	2.73	8.37	10.2
Eu	1.30	1.28	0.61	0.85	0.87	0.68	0.70	0.64	0.63	0.32	0.21	0.57	0.73
Gd	4.58	4.99	6.47	8.26	9.06	6.75	6.31	7.93	8.50	5.63	2.98	7.85	10.7
Tb	0.65	0.71	0.89	1.39	1.50	1.06	0.99	1.33	1.41	1.18	0.60	1.43	1.97
Dy	3.68	4.09	4.77	8.44	8.77	6.24	5.65	8.31	8.94	8.26	4.19	9.44	11.8
Ho	0.75	0.78	0.94	1.64	1.75	1.22	1.09	1.71	1.81	1.83	0.86	1.95	2.29
Er	2.14	2.24	2.75	4.93	5.28	3.58	3.24	5.20	5.60	5.85	2.84	6.18	6.78
Tm	0.31	0.33	0.41	0.73	0.79	0.52	0.51	0.79	0.85	0.97	0.48	0.95	1.02
Yb	2.17	2.20	2.73	4.98	5.21	3.52	3.37	4.88	5.73	6.89	3.33	6.54	6.80
Lu	0.35	0.36	0.43	0.75	0.78	0.54	0.52	0.73	0.87	1.07	0.53	0.97	1.02
Be	5	5	3	8	8	7	7	5	6	6	8	5	11
M	1.47	1.49	1.34	1.44	1.43	1.38	1.43	1.38	1.32	1.38	1.33		
T_{Zr} (°C)	813	797	711	757	761	776	753	748	763	670	661		

T_{Zr} (°C)—zircon saturation temperature estimate in °C calculated according to Boehnke et al. (2013); M = (Na + K + 2Ca)/(Al × Si).

TABLE 2 | Nd isotopic composition of granitic rocks of the TSP and BU intrusions.

Sample	Age (Ma)	Phase	Nd (ppm)	Sm (ppm)	$^{147}Sm/^{144}Nd$	$^{143}Nd/^{144}Nd_{(m)}$	2σ	$^{143}Nd/^{144}Nd_{(i)}$	$\varepsilon_{Nd(t)}$	T_{DM} (Ma)
WOL-12	191	1	32.94	5.43	0.0998	0.512560	6	0.512435	0.84	659
WOL-12–1	191	1	39.11	6.68	0.1033	0.512548	6	0.512419	0.52	695
WOL-14	183	2	40.25	8.75	0.1314	0.512558	7	0.512401	−0.04	905
WOL-15	183	2	41.37	8.42	0.1231	0.512568	8	0.512421	0.35	809
BU-1	221		26.3	6.75	0.1552	0.512648	6	0.512424	1.37	1032
BU-5	221		42.6	9.82	0.1394	0.512631	6	0.512429	1.48	849
BU-9	221		23.2	5.27	0.1373	0.512631	8	0.512432	1.54	832
BU-13	221		17.3	4.23	0.1478	0.512642	6	0.512428	1.46	934
BU-16	221		7.2	1.39	0.1167	0.512609	6	0.512440	1.69	695
BU-19	221		28.8	7.24	0.152	0.51265	6	0.512433	1.55	976
BU-25	221		27.2	5.39	0.1198	0.512642	6	0.512468	2.23	667
BU-34	221		44.5	9.01	0.1224	0.512617	6	0.512440	1.69	724

T_{DM}—depleted mantle model age calculated using the model of DePaolo (1988). $\varepsilon_{Nd}(t)$—age-corrected values calculated for the respective crystallization age; $^{143}Nd/^{144}Nd_{(m)}$—measured value; and $^{143}Nd/^{144}Nd_{(i)}$—initial, calculated, age-corrected. TSP: WOL samples; BU: Bayan-Ulan samples—data from Dostal et al. (2015b).

intensities of ^{238}U were left unchanged, if measured in a counting mode, and recalculated from ^{235}U intensities, if the ^{238}U was acquired in analog mode. No common Pb correction was applied to the data due to the high Hg contamination of the commercially available He carrier gas, which precludes accurate correction of the interfering ^{204}Hg on the very small signal of ^{204}Pb (common lead). The Hg impurities in the carrier He gas were reduced by using an in-house made gold-coated sand trap.

Elemental fractionation and instrumental mass bias were corrected by the normalization of an internal natural zircon reference material Plešovice for samples WOL-12 and WOL-14 (337 Ma, Sláma et al., 2008) and 91500 (1065 Ma, Wiedenbeck et al., 1995) for sample WOL-15. Zircon reference materials GJ-1 (609 Ma, Jackson et al., 2004; 603 Ma, Kylander-Clark et al., 2013) were periodically analyzed during the measurement for quality control, and the values for the natural standard correspond well and are less than 1.5% accurate within the published reference values. Raw data reduction and age calculations, including corrections for baseline, instrumental drift, mass bias, and down-hole fractionation, were carried out using the computer program Iolite (v. 3.5; Paton et al., 2011) with the VizualAge utility (Petrus and Kamber, 2012). All presented ages are quoted at 2σ absolute. The discordance limit for the concordant population was taken as 1.5% (**Supplementary Table S1**) and was calculated as follows: $D < 1\text{Ga} = [1 - (((^{206}Pb/^{238}U)/(^{207}Pb/^{235}U))] \times 100$.

GEOCHRONOLOGY

The age of the TP was not well established. The K-Ar whole-rock dating for the granite of the TP yielded a cooling age of 190.5 ± 4.7 Ma, whereas the whole-rock Rb-Sr gave an age range of 225 to 188 Ma (Smirnov et al., 1977). In order to refine the age, we have dated the pluton by a U-Pb zircon laser ablation ICP-MS technique.

The U-Pb isotopic ratios in zircons were measured in three samples (see **Supplementary Table S1** and **Figure 5** for dating results). Sample WOL-12 is biotite granite from the first intrusive phase while samples WOL-14 and WOL-15 are biotite granites from the second intrusive pulse. Most of the zircon grains from WOL-12, WOL-14, and WOL-15 are slightly pale brown or clear and are predominantly prismatic grains, and their fragments or rarely needles have a length of ∼200 to 500 μm. Internal crystal interiors visible in CL imaging revealed that the most of crystals show well-developed magmatic oscillatory (or sector) zoning with only slight alteration with rare featureless unzoned cores (**Figure 6**). All studied samples show uniform Th/U 0.1–0.6 (average value of 0.4; see **Supplementary Table S1**) in both the rims and cores. This Th/U ratio is typical of a magmatic origin (Hoskin and Schaltegger, 2003 and references therein).

U-Pb zircon dating of sample WOL-12 yielded a scatter in concordant ages between c. 185 Ma and 195 Ma that constitute a single concordia age of *c*. 191 ± 2 Ma (2σ; 25 analyses; **Figure 5**). The majority of zircon crystals extracted from samples WOL-14 and WOL-15 yielded a well-defined concordia magmatic age of ∼183 ± 2 Ma (2σ; 25 analyses; **Figure 5**) and 183 ± 2 Ma (2σ; 21 analyses; **Figure 5**), respectively. Inherited ages do not significantly differ from those obtained in zircon domains with magmatic growth zoning (**Figure 6**). Thus, the first phase intruded at ∼191 Ma while the second phase was emplaced at ∼183 Ma.

GEOCHEMISTRY

Sampling and Alteration

The analyzed set of representative samples from TP pluton (**Table 1**) consists of two biotite granites (WOL-12 and WOL-12-1) and an aplite (WOL-13-1) from the first intrusive phase, four biotite granites (WOL-14,WOL-14-1, WOL-15, and WOL-15-1), two leucogranites (WOL-6 and WOL-10), and two moderately altered leucogranites (WOL-4 and WOL-5) of the second intrusive phase and two strongly altered granitic samples (WOL-7 and WOL-8).

The chemical compositions of the biotite granites were not significantly modified by secondary processes. On the other

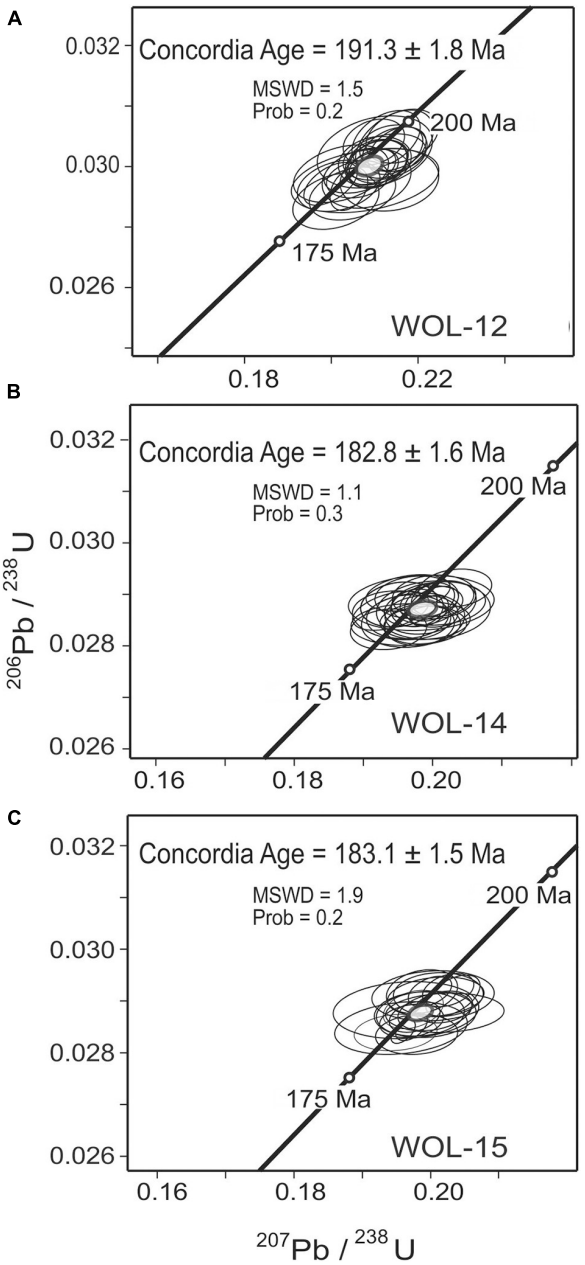

FIGURE 5 | Concordia diagrams with U-Pb isotopic data of studied samples **(A)** WOL-12, **(B)** WOL-14, and **(C)** WOL-15. All ages are quoted with 2σ uncertainties.

hand, there are notable differences among the leucogranites. Leucogranites (WOL-6 and WOL-10) probably retained most of their original composition while the moderately altered leucogranites (WOL-4 and WOL-5) were silicified, leading mainly to an addition of silica. The other two samples (WOL-7 and WOL-8) were strongly hydrothermally altered and accompanied by a notable change of the chemical composition. These two samples were not consequently plotted on some diagrams.

In addition to the TP rocks, 12 samples from the Bayan-Ulan granitic intrusion (see section "Relationship between petrogenesis and mineralization") were also analyzed (**Supplementary Table S2**). These samples do not appear to be noticeably affected by secondary processes (Dostal et al., 2015b).

Major and Trace Elements

The granitic rocks of the TP are highly siliceous and fractionated with silica contents ranging from 71 to 77 wt.% (**Figure 7**). The silica contents of the first intrusion vary between 72 and 75 wt.% in contrast to the second phase with 71 to 77 wt.%. On the normative quartz-alkali feldspar-plagioclase (QAP) graph (**Figure 8A**), they plot into the field of granite. Although there are differences between the two intrusive phases, all the rocks have molar $Al_2O_3/(Na_2O + K_2O) \sim 1–1.2$ and $Al_2O_3/(CaO + Na_2O + K_2O) \sim 1$, indicative of their mildly peraluminous character with the exception of the granites of the first phase, which are mildly metaluminous (**Figure 8B**). The granites also have a high $FeO^*/(FeO^* + MgO)$ ratio (**Figure 7A**) and correspond to ferroan granites of Frost and Frost (2011). According the modified alkali-lime index [MALI = $(Na_2O + K_2O\text{-}CaO)$] of Frost and Frost (2011), the rocks are mostly alkali-calcic (**Figure 7B**); the granites also have high contents of K_2O (**Figure 7C**). The variations of major and several trace elements relative to silica (**Figure 7**), particularly for the second phase, indicate that the granites underwent fractional crystallization. The TP granites, particularly those of the first phase, are comparable to those of numerous other intrusions of the Khentei batholith (Yarmolyuk et al., 2013).

The chondrite-normalized REE patterns of all the studied granites are enriched in light REE (LREE) and have relatively flat unfractionated heavy REE (HREE) and negative Eu anomalies. However, there are subtle differences among the rocks of the two intrusive phases. The patterns of phase 1 (**Figure 9**) have a relatively high $(La/Yb)_n$ ratio (∼14–18) accompanied by $(La/Sm)_n \sim 4$ to 6 and slightly sloping HREE with low $(Gd/Yb)_n$ ratios (∼1.8). They are closely comparable to the average of the granitic rocks of the whole Khentei batholith (**Figure 9**) reported by Yarmolyuk et al. (2013). The second intrusive phase has patterns with $(La/Yb)_n$ ranging from ∼7 to ∼10 and a more pronounced negative Eu anomaly than the first intrusive pulse. The leucogranites of the second pulse have variable REE patterns including a nearly flat one with $(La/Yb)_n \sim 1.2$ and $(Gd/Yb)_n \sim 0.7$. The altered leucogranites have patterns comparable to those of leucogranites. The flat HREE patterns imply that garnet was not in the source of the granites.

The primitive mantle-normalized plots of the TP granites (**Figure 10**) are distinctly enriched in several large ion lithophile elements, namely, Cs, Rb, Th, and U and depleted in Ba, Sr, Eu, Nb, and Ti. The altered leucogranites also have distinct positive anomalies for W and Sn. Relative to the granites of the first phase, the second-phase granites have lower Ba and Sr (**Figure 7**) but higher Rb, Ta, W, and Sn (**Figure 10**). An enrichment of Rb in the second-phase granites is reflected by the relatively low K/Rb ratio (mostly 50–150) compared to typical crustal values of ∼230

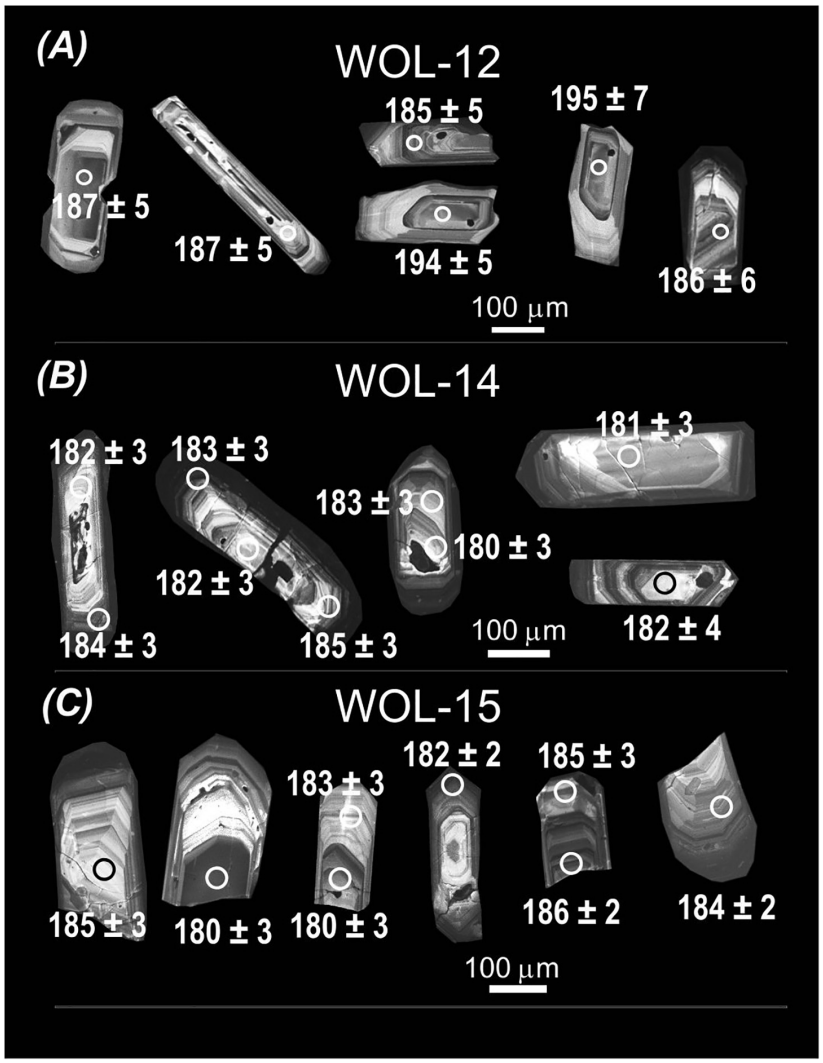

FIGURE 6 | Representative cathodoluminescence images of the dated zircons grains. The spots (25 μm) where laser ablation analysis was performed are indicated together with obtained $^{206}Pb/^{238}U$ ages in Ma (±2σ uncertainties). **(A)** zircons from sample WOL-12; **(B)** zircons from sample WOL-14; **(C)** zircons from sample WOL-15.

(Shaw, 1968; Taylor and McLennan, 1985). These rocks also have anomalous Ba/Rb and Rb/Sr ratios.

The temperatures of zircon saturation (T_{Zr}), estimated from relating the concentration of Zr to the bulk composition of the magma (Watson and Harrison, 1983; Hanchar and Watson, 2003; Boehnke et al., 2013), are variable for the various TP rocks (**Table 1**). The average temperature estimates range from a relatively high value (∼805°C) for the granites of the first phase through the granites of the second phase (∼762°C) and leucogranites (∼755°C) to low values for the moderately altered leucogranites (∼665°C) and aplite (∼710°C).

Nd Isotopes

The Nd isotopic data are given in **Table 2**. The initial isotopic ratios and $\varepsilon_{Nd}(t)$ values are age-corrected to the ages of the emplacement (phase 1 = 191 Ma; phase 2 = 183 Ma). $\varepsilon_{Nd}(t)$ values of the TP granitic rocks are close to chondritic values (0 to +0.8), indicating that they were derived from a reservoir with a long-term history of near-chondritic Sm-Nd values. The values are similar to those of Jahn et al. (2009) for the Early Mesozoic A-type granitoid rocks from this part of the CAOB (0 to +4) and are within the range of the granitoids of the Khentei batholith (+2 to −4; Yarmolyuk et al., 2013). The Nd model ages (T_{DM}) ranging from 650 to 900 Ma suggests a Neoproterozoic source.

DISCUSSION

Petrogenesis

According to the chemical composition, the TP granitic rocks correspond to the A-type granites (**Figure 11A**). Specifically, they resemble the A2 group (*sensu* Eby, 1992),

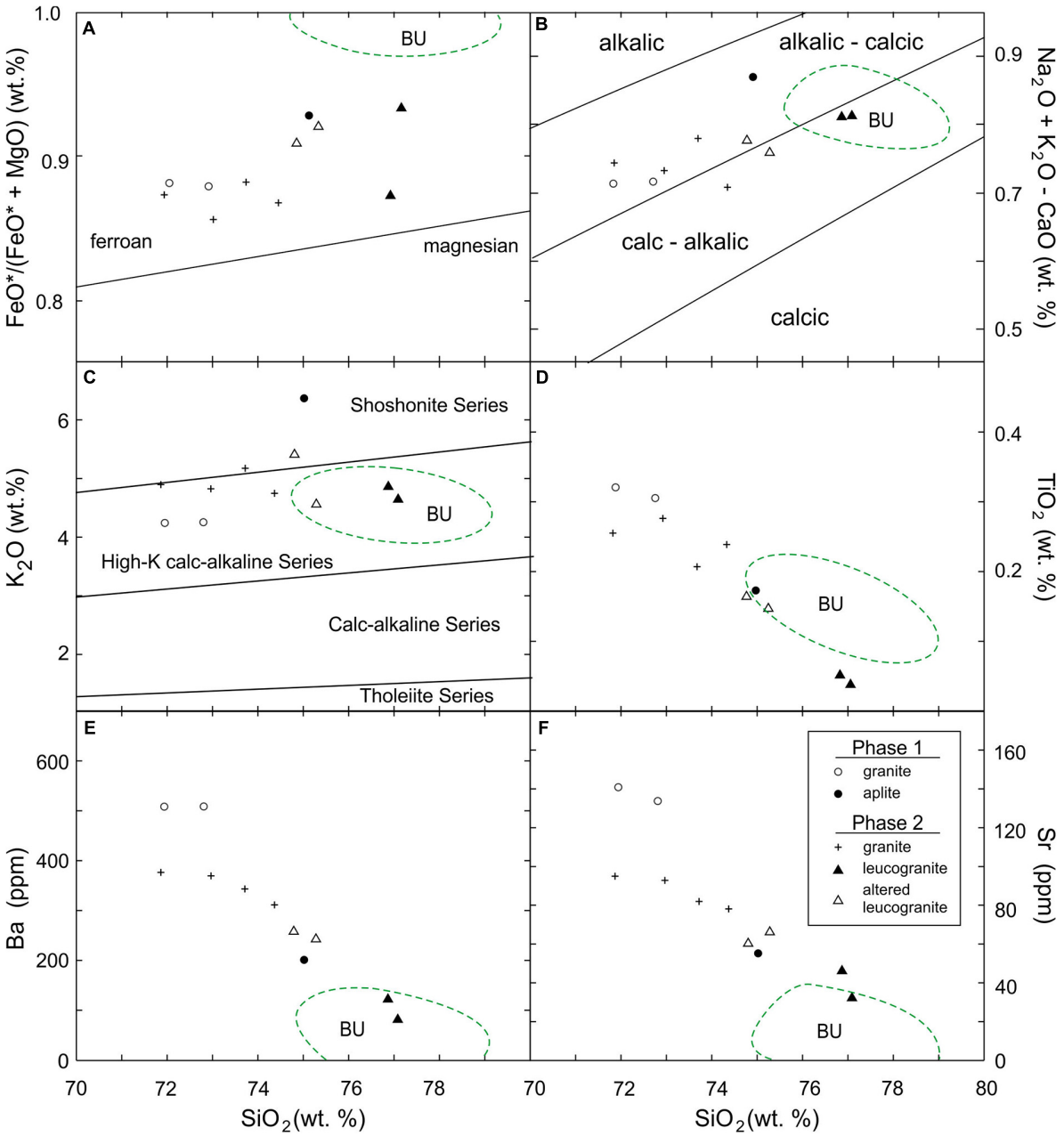

FIGURE 7 | Variations of SiO_2 (wt.%) versus **(A)** FeO*/(FeO*/MgO) showing the separation of ferroan and magnesian suites based on the relative degree of iron enrichment during differentiation (after Frost and Frost, 2011). **(B)** Modified alkali-lime index (MALI = $Na_2O + K_2O$-CaO) with fields defined by Frost and Frost (2011). **(C)** K2O (wt.%) with fields after Peccerillo and Taylor (1976). **(D)** TiO_2 (wt.%), **(E)** Ba, and **(F)** Sr (ppm) in the granitic rocks of the Tukham pluton. Dashed green curves outline the field (BU) for the Bayan-Ulan pluton.

which typically represents magmas derived from lower to middle continental crust, or underplated crust (**Figure 11B**). These characteristics are consistent with their ferroan and alkali-calcic features (Frost and Frost, 2011). Collectively in the TP granites, TiO_2, FeO*, Al_2O_3, MgO, CaO, P_2O_5, Ba, and Sr decrease with increasing SiO_2 (**Figure 7**), indicating crystallization of plagioclase, ferromagnesian minerals (biotite), and accessories (Fe-Ti oxides and apatite). Negative anomalies of Sr, Ba, Eu, Nb, and Ti on the primitive mantle normalized plots also support such a process (**Figure 10**). Covariations of Ba versus Sr (**Figure 12**) indicate that the fractionation of feldspars played a major role during the magma evolution. However, the TP granitic rocks represent two magma pulses derived from distinct sources at different times. While the rocks of the first intrusion closely resemble the average composition of the Khentei batholith,

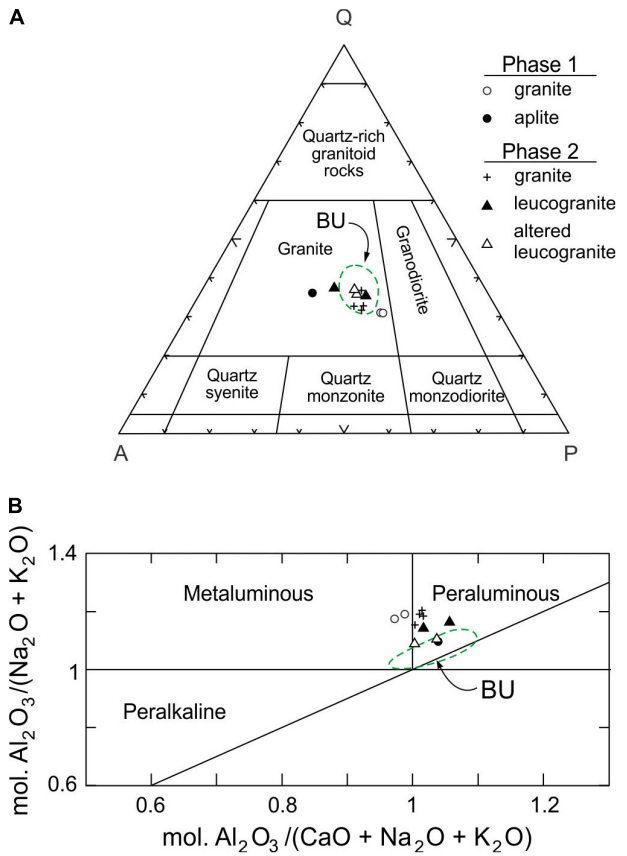

FIGURE 8 | (A) Mesonormative quartz-alkali feldspar-plagioclase (QAP) ternary classification diagram used to characterize the modal composition of the plutonic rocks. It shows the Tukhum granitic rocks whereas the dashed green curve outlines the field (BU) for the Bayan-Ulan pluton. **(B)** $Al_2O_3/(Na_2O + K_2O)$ versus $Al_2O_3/(CaO + Na_2O + K_2O$; in mole%) diagram for TP granitic rocks defining the ranges of peraluminous, metaluminous, and peralkaline plutonic rocks. The dashed green line delineates the field (BU) for the rocks from Bayan-Ulan pluton.

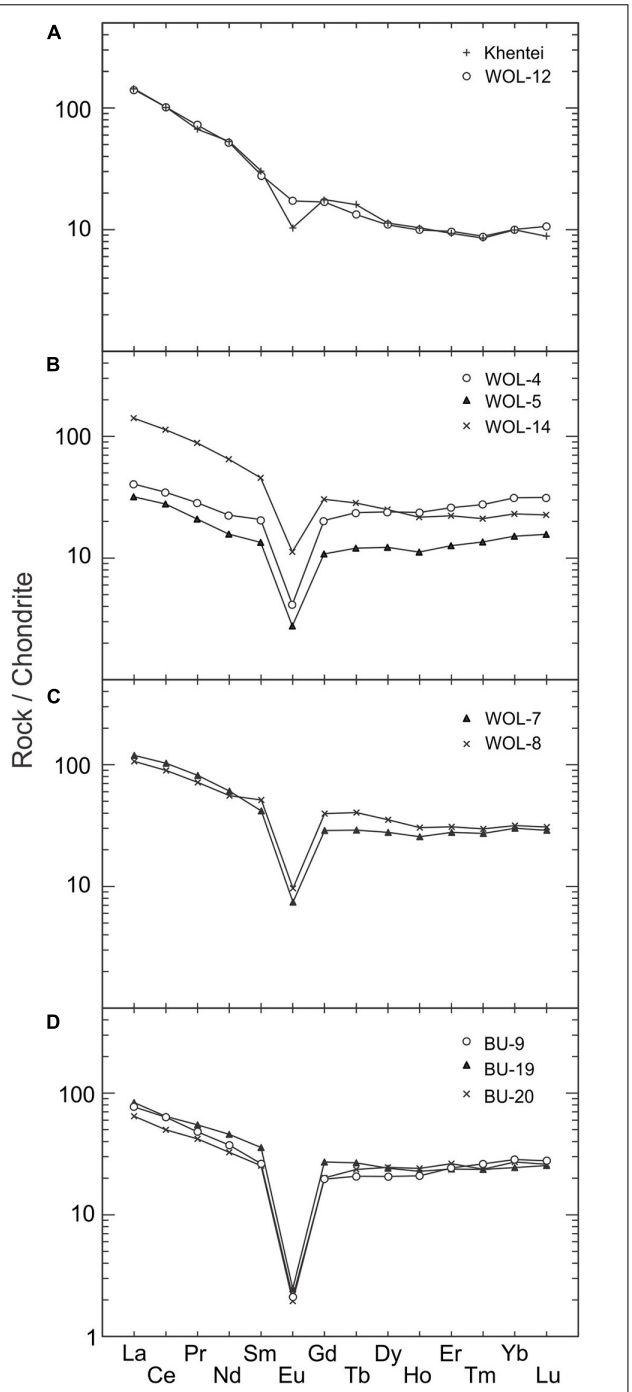

FIGURE 9 | Chondrite-normalized rare-earth element diagrams for **(A)** phase 1 TP granite (WOL-12) and the average of granitic rocks of the Khentei batholith (Yarmolyuk et al., 2013); **(B)** phase 2 TP granites (WOL-14 typical biotite granite; WOL-4 and 5-altered leucogranites); **(C)** TP strongly altered granites; and **(D)** granites of the Bayan-Ulan pluton. Normalizing values are after Sun and McDonough (1989).

the granites of the second phase have different geochemical characteristics (including T_{Zr}) and underwent more extensive fractional crystallization.

The origin of A2-type granitic rocks has been typically attributed to either fractional crystallization or crustal melting (Eby, 1992; Bonin, 2007). These processes can also be invoked for the generation of the TP granitic rocks, which intruded during the last stages of the emplacement of the Khentei batholith and of the plutons of the rift zones surrounding the megadome. More specifically, the petrogenetic processes are (1) extensive fractional crystallization of a mantle-derived mafic or intermediate magma with or without crustal contamination and (2) partial melting of middle or lower crustal source rocks.

Compositional similarities of the granites of the first intrusion to the average of the Khentei batholith and to an estimate of the total crust of East China (**Figures 9**, **10**), peraluminous/metaluminous characteristics of the granitic rocks, and the lack of intermediate rock types (Daly gap) negate an origin by fractional crystallization of mantle-derived mafic or intermediate magma but are consistent with a process where rising mafic magma triggers partial melting of the crustal material

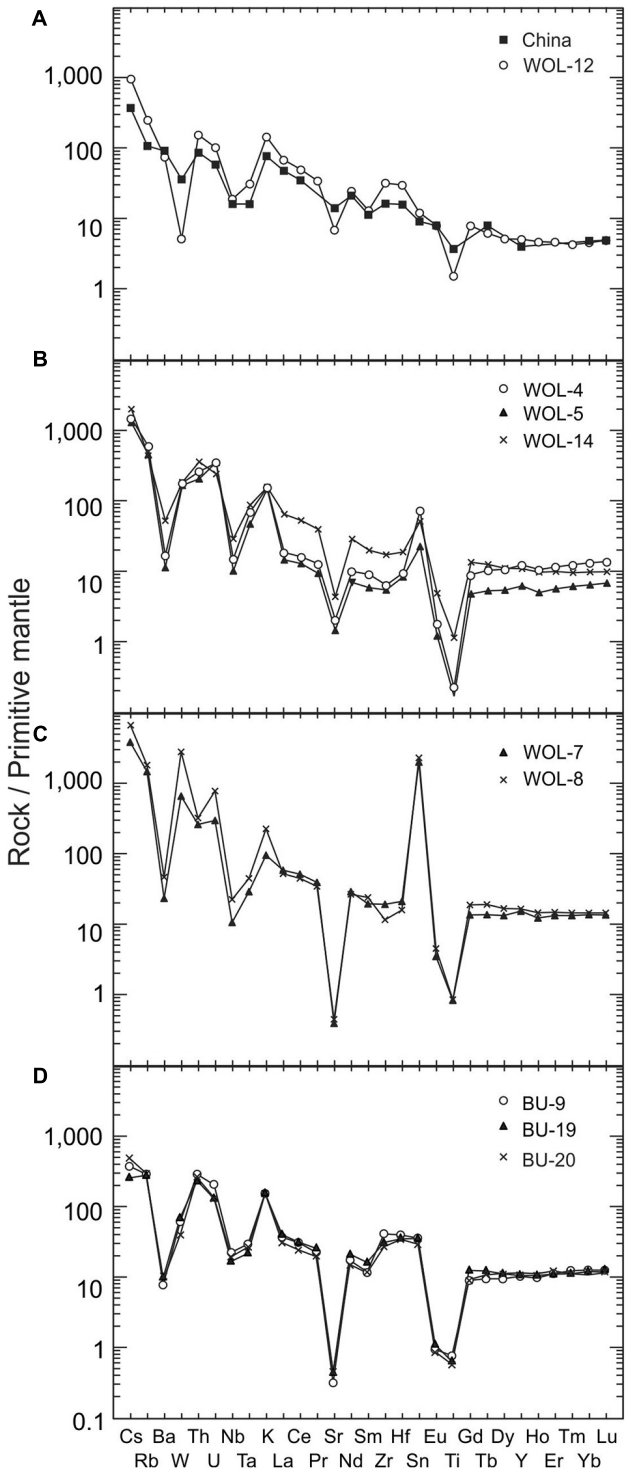

FIGURE 10 | Primitive-mantle normalized incompatible element abundances for the granitic rocks of the Tukham and Bayan-Ulan plutons. **(A)** Phase 1 TP granite (WOL-12) and an estimate of total crust of Eastern China (Gao et al., 1998); **(B)** phase 2 TP granites (WOL-14 typical biotite granite; WOL-4 and WOL-5 altered leucogranites); **(C)** TP strongly altered granites; and **(D)** granites of the Bayan-Ulan pluton. Elements are arranged in the order of decreasing incompatibility from left to right. Normalizing values are after Sun and McDonough (1989).

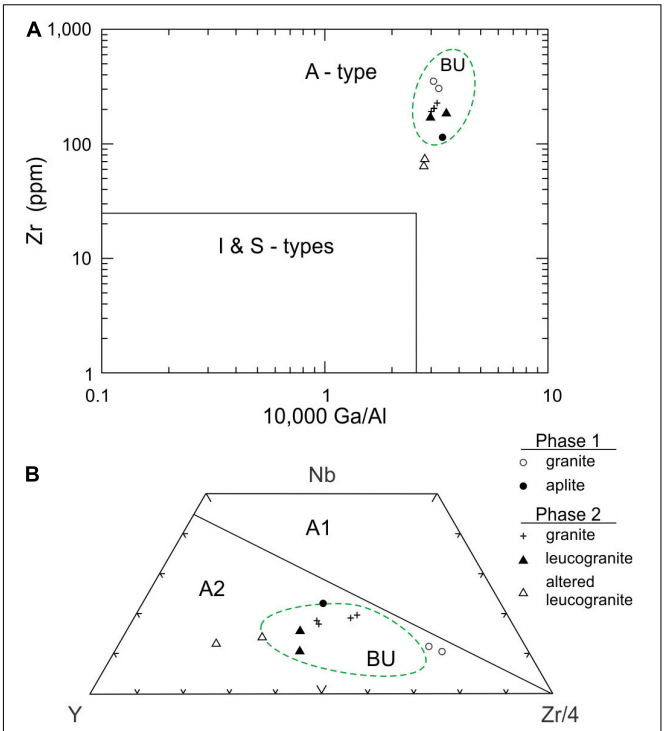

FIGURE 11 | (A) Plot of 10^4 Ga/Al versus Zr (ppm) of Whalen et al. (1987) showing the A-type characteristics of the granitic rocks of the Tukham pluton. I and S field is for I- and S-type granites. **(B)** Y-Nb-Zr/4 diagram of Eby (1992) for the granitic rocks of the Tukham pluton showing the fields of the A1 and A2 granitoids. The dashed green curves show the fields (BU) for the Bayan-Ulan pluton.

from which the granitic magma inherit their geochemical characteristics. This is a common process during lithospheric extension and is a consequence of magmatic underplating and crustal melting (e.g., Huppert and Sparks, 1988). Thus, the TP granites are probably the results of partial melting of the middle/lower crust of granodioritic–tonalitic composition (cf. Frost and Frost, 2011). The Nd model ages (**Table 2**) suggest that the sources were of Neoproterozoic age. The differences in the T_{Zr} between the two intrusive phases reflect, in part, different melting conditions. The low T_{Zr} (<800°C) of felsic magma of the second phase is considered to reflect water-fluxed melting as opposed to the relatively high temperature (>800°C) during anhydrous melting of magma of the first phase (Miller et al., 2003; Collins et al., 2016). The low T_{Zr} for the mineralized leucogranites (~665°C) is probably due to the activities of fluids.

Relationship Between Petrogenesis and Mineralization

The petrogenesis of peraluminous fluorine-rich leucogranites such as those of TP is still under dispute, although these rocks can be associated with Sn-W-U-Ta mineralization (Linnen, 1998; Černý et al., 2005; Linnen and Cuney, 2005). These rocks are enriched in incompatible trace elements such as Rb, Cs, Th, U, W, and Sn and depleted in Ti, Ba, Sr, Nb, and Eu. They also

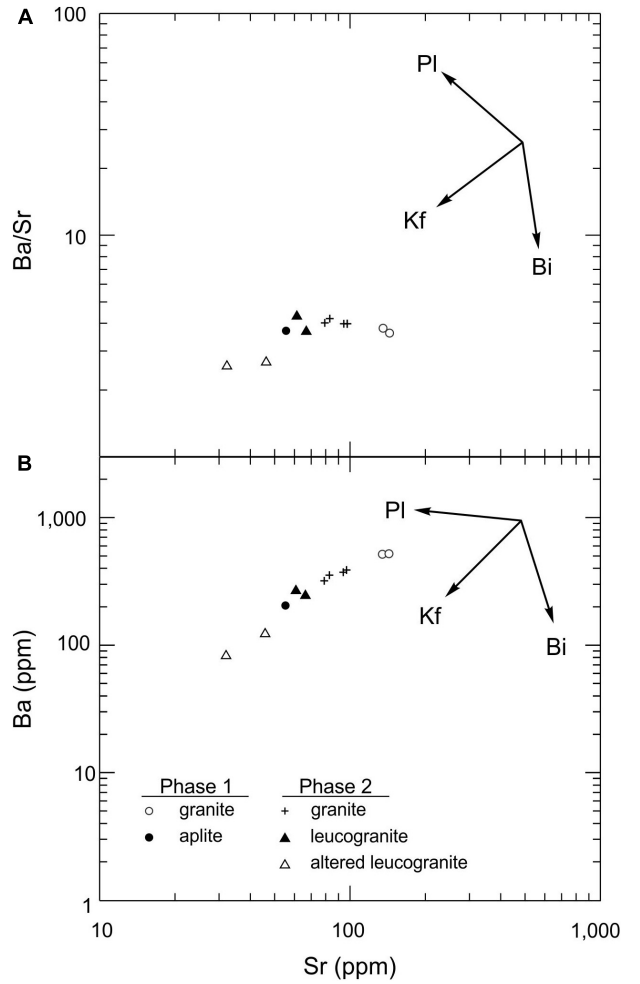

FIGURE 12 | (A) Ba/Sr and **(B)** Ba versus Sr (in ppm) diagrams for the granitic rocks of the Tukham pluton. Vectors depict the fractionation trends of the compositional changes in the residual liquid when the specified phase is progressively removed from the magma during fractional crystallization; Pl—plagioclase; Kf—K-feldspar; and Bi—biotite.

have unusual mineralogical characteristics, such as the presence of topaz and fluorite. These rocks commonly represent the late phase of late-orogenic or anorogenic granite plutons. Two main genetic hypotheses are magmatic and metasomatic, i.e., whether their geochemical characteristics are due to magmatic processes or to post-magmatic fluid–rock interaction. Furthermore, if the characteristics are due to magmatic activities, then the chemical composition could reflect either a distinct source or unusual evolution, involving, e.g., fluorine-rich fluids.

The smooth variation trends for some major and trace elements of the granites and leucogranites of the second intrusion (**Figure 7**) and their similarities to those from non-mineralized plutons indicate that most of the chemical compositions reflect primary magmatic evolution, including extensive fractional crystallization. On the other hand, the enrichment of some elements such as Rb (accompanied by low K/Rb), a kinked shape REE pattern, and the occurrence of topaz and fluorite among others probably reflect fluid fractionation/interaction involving fluorine. This suggests that trace elements in some rocks were modified by late or post-magmatic fluid–rock interaction (Webster et al., 2004; Salvi and Williams-Jones, 2005; Thomas et al., 2005; Dostal et al., 2015a). The petrographic observations (such as the presence of various pseudomorphs and replacement textures; Ivanova, 1976) also indicate that mineral assemblages of the leucogranites are the results of both magmatic processes as well as late- or post-magmatic fluid–melts interactions. The interaction of the leucogranites with fluids led to the enrichment and redistribution of several incompatible trace elements but has not modified their major and some trace element composition. These highly evolved melts commonly moved/escaped into the apical part of the pluton along the fracture zones and are now represented by the leucogranites.

The experimental studies (e.g., Syritso et al., 2018) indicate that the W preferentially partitions into the fluid phase, which commonly escapes from a magma chamber to the host rocks forming wolframite-bearing quartz veins or greisen that are typically structurally controlled. Their frequent association with fractionated granites indicates that they are closely related, although the W mineralization is post-magmatic and related to the hydrothermal solutions. They were probably derived from the same highly fractionated magma chamber. The W mineralization is also associated with greisen. Greisen represents granites, which were altered by fluids released from the magma during the late stages of its evolution. The geochronological study of Syritso et al. (2018) on several similar tungsten deposits from eastern Transbaikalia concluded that tungsten mineralization took place almost synchronously with the crystallization of associated granites. It also appears that in this part of CAOB including TP, the W mineralization is related mainly to Mesozoic plutons, where it was emplaced along the faults in apical parts of intrusions (Syritso et al., 2018).

Comparison With Granites of the Rift Zones

To evaluate the differences between the granitic rocks of the TP, a representative intrusion of the Khentei batholith, and those of the rift zones, the TP rocks are compared with those of the Bayan-Ulan pluton (221 Ma; Dostal et al., 2015b) from the North Gobi rift zone (**Figure 2**). For comparison, which might also reveal a contrast between the ore-bearing and barren granites, we have augmented the Bayan-Ulan whole-rock analyses of Dostal et al. (2015b) with the new data (**Supplementary Table S2**). The Bayan-Ulan pluton (BU), located about 200 km east of Ulaanbaatar, outcrops over an area of ∼1000 km^2. The intrusion (Dostal et al., 2015b) is composed mainly of coarse-grained leucocratic granite containing mesoperthite with interstitial quartz and minor to trace amounts of Fe-rich alkali amphiboles and, rarely, Fe-rich biotite. The granites have relatively uniform chemical compositions; they are highly fractionated alkaline A2-type granites with silica ranging from 75 to 78.5 wt.% (**Figure 7**). Compared to the TP, the BU granites are lower in MgO, CaO, and MnO but have a higher FeO*/(FeO* + MgO) ratio (>0.95). They are predominantly peraluminous (**Figure 8**). Chondrite-normalized REE plots display a slight LREE enrichment with $(La/Yb)_n$ ∼ 2–7 and a

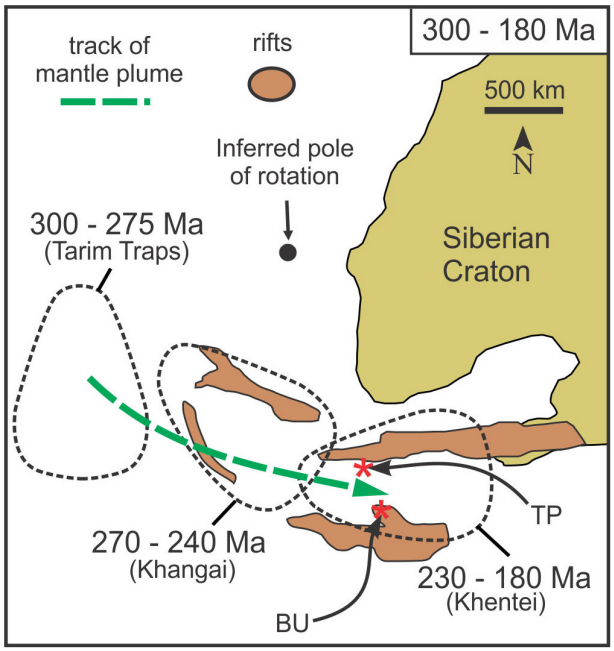

FIGURE 13 | Reconstruction of the movement of the Mongolian mantle plume and the location of the magmatic complexes in northern Mongolia and Transbaikalia (modified after Yarmolyuk and Kuzmin, 2011, 2012; Dostal et al., 2014). Dashed lines show the migration of magmatism and the positions of the Mongolian plume at 300 to 275 Ma, 270 to 240 Ma, and 230 to 180 Ma. The arrow is a tracer of Mongolian plume. TP—Tukhum pluton; BU—Bayan Ulan pluton.

distinct negative Eu anomaly (**Figure 9**). The primitive mantle-normalized patterns (**Figure 10**) are enriched in Th, U, and Rb and relatively more depleted in Ba, Sr, Eu, and Ti. Most BU granites have $\varepsilon_{Nd}(t)$ values of +1.4 to +1.7 and T_{DM} model ages ~650–1050 Ma (**Table 2**). Whereas the BU model ages overlap those of TP rocks, their $\varepsilon_{Nd}(t)$ are higher. The BU rocks were derived from a different source and underwent a different fractionation path. Dostal et al. (2015b) inferred that they were formed by the partial melting of underplated Neoproterozoic mildly alkaline basalts in the lower crust, followed by fractional crystallization. In addition, the fluids and fluid fractionation played a significantly smaller role during the evolution of the BU intrusion compared to the TP. The main Fe-Mg mineral in the BU rocks is alkali amphibole, while in the TP rocks, it is biotite. The BU rocks are not associated with a W or Sn mineralization. A comparison of the three intrusions (two TP pulses and BU) implies that the granites hosting rare metal mineralization required a distinct crustal source enriched in these elements, a high degree of fractionation, and an involvement of fluorine-rich fluids during their evolution.

Tectonic Implications

After the collision of the Siberian and North China cratons, which led to the closure of the Mongol-Okhotsk basin, north-central Mongolia and an adjoining part of southern Siberia (eastern Transbaikalia) witnessed, during the Late Permian to Early Jurassic, an emplacement of large, concentrically zoned magmatic structures. One of these magmatic structures is the Khentei (Daurian-Khentei) megadome (**Figure 2**).

The emplacement of the A2-type granitic plutons of the Khentei batholith and of the surrounding rift zones is related to rifting and partial melting. The origin of the granitic rocks requires a heat source to produce an elevated temperature. Such a heat source is usually attributed to one of the following processes: (1) delamination of the lower lithosphere, (2) thinning of lithosphere during rifting, and (3) rising of a mantle plume. The application of these tectonic models to the region has been under discussion (e.g., Yarmolyuk and Kuzmin, 2011; Donskaya et al., 2013; Li et al., 2013). We favor the mantle plume as the heat source for magmatic activities in the area as it explains well the spatial and temporal variations in Eastern Mongolia and Transbaikalia, particularly the eastward movement of large-scale magmatism over time. Yarmolyuk and Kuzmin (2011) and Dostal et al. (2014) among others noted the eastward migration of the magmatic centers through time from the Tarim traps (300–275 Ma; >250,000 km^2) through the Khangai magmatic center at 270 to 240 Ma to the Khentei (230–183 Ma) in central Mongolia (**Figure 13**). The Tarim traps are Permian continental flood basalts, which form a main part of the Tarim Large Igneous Province located in the Tarin Basin. The migration of the magmatic activities is consistent with the movement of Mongolia over a stationary mantle plume (Mongolian plume of Kuzmin et al., 2010; Yarmolyuk and Kuzmin, 2011) and is supported by paleomagnetic data (Kuzmin et al., 2010).

The plume model can also account for the zonal arrangement of the Khentei magmatic center ranging from granites and granodiorites in the core of the batholith through Li-F-rich granites along the margin of the batholith (either within or just outside of the batholith) and finally to alkaline and peralkaline lavas and alkaline granitoid intrusions in the outer margin of the rifts (Yarmolyuk and Kuzmin, 2011). A larger degree of melting that took place at a shallower depth above the core of the magmatic center generated granites, while a deeper and smaller degree of melting took place at the margins and produced alkaline and peralkaline rocks.

CONCLUSION

The TP, one of the constituent bodies of the Mesozoic Khentei batholith, is made up of two distinct intrusions dated at ~191 and 183 Ma, suggesting that the magmatic activity of the batholith lasted longer than the range of 230 to 195 Ma proposed by Yarmolyuk and Kuzmin (2011). The TP rocks are silica-rich A2-type granites, which are mainly alkali-calcic. On the primitive mantle normalized plots, they are enriched in Rb, Cs, U, and Th and depleted in Ba, Sr, Eu, Nb, and Ti. The TP rocks have $\varepsilon_{Nd}(t)$ ~ 0 to +1 and Nd model ages ~650–900 Ma. The isotopic values are within the range of other Mesozoic granites of the Khentei batholith. The granites were derived by the partial melting of middle/lower crustal Neoproterozoic rocks, followed by fractional crystallization. However, the presence of F-rich minerals in the rocks of the second intrusion as well as W-Sn

mineralization suggests that the source of the parent magma of this intrusion was enriched in several rare metals including W and Sn. The younger second intrusion also contains leucogranites with trace element compositions indicative of combined crystal and fluid fractionation during the late stages of the evolution. The bulk of the tungsten mineralization of the TP is hosted in quartz veins and resulted from an escape of fluids from a magma chamber. The mineralization is associated with the evolution of the granitic magma. An increase of the pressure of the fluids in the magma chamber and their escape caused a brecciation of the rocks and triggered an emplacement of quartz veins hosting the W mineralization.

The partial melting required a heat source. The Late Paleozoic to Early Mesozoic granitic province in north-central Mongolia, which includes two batholiths, Khangai and Khentei, and the eastward migration of the magmatic center through time, is consistent with a mantle plume as a heat source for magmatism. The eastward migration of the magmatic centers over time from the Tarim Large Igneous Province (South Mongolia-Tarim traps) at 300–275 Ma through the Khangai magmatic center with the Khangai batholith at 270–240 Ma to the Khentei area of Eastern Mongolia and Transbaikalia (230–180 Ma) can be explained by the movement over a stationary mantle plume (the Mongolian plume of Yarmolyuk and Kuzmin, 2011).

DATA AVAILABILITY STATEMENT

All datasets generated for this study are included in the article/**Supplementary Material**.

AUTHOR CONTRIBUTIONS

JD developed the idea, wrote the bulk of the manuscript, processed data, and collected samples. MS wrote a part of the manuscript, processed data, and created figures. OG contributed to the ideas and concept and wrote a part of the manuscript. RC collected and prepared samples and created figures. All authors contributed to the article and approved the submitted version.

FUNDING

This study was supported by NSERC Canada Discovery grant to JD and by the institutional support RVO67985831 to MS.

ACKNOWLEDGMENTS

We thank reviewers Ali Polat and Changqian Ma and co-editor Greg Shellnutt for constructive reviews that significantly improved the manuscript. We are also grateful to Yo. Majigsuren for providing assistance during fieldwork and for field photos and to J. Batsukh for help with a map compilation.

SUPPLEMENTARY MATERIAL

The Supplementary Material for this article can be found online at: https://www.frontiersin.org/articles/10.3389/feart.2020.00242/full#supplementary-material

REFERENCES

Antipin, V., Gerel, O., Perepelov, A., Odgerel, D., and Zolboo, T. (2016). Late Paleozoic and Early Mesozoic rare-metal granites in Central Mongolia and Baikal region: review of geochemistry, possible magma sources and related mineralization. *J. Geosci.* 61, 105–125. doi: 10.3190/jgeosci.211

Baker, T., Pollard, P. J., Mustard, R., Markl, G., and Graham, J. L. (2005). A comparison of granite-related tin, tungsten and gold-bismuth deposits: implication for exploration. *SEG Newslett.* 61, 5–17.

Boehnke, P., Watson, E. B., Trail, D., Harrison, T. M., and Schmitt, A. K. (2013). Zircon saturation revisited. *Chem. Geol.* 351, 324–334. doi: 10.1016/j.chemgeo.2013.05.028

Bonin, B. (2007). A-type granites and related rocks: evolution of a concept, problems and prospects. *Lithos* 97, 1–29. doi: 10.1016/j.lithos.2006.12.007

Černý, P., Blevin, P. L., Cuney, M., and London, D. (2005). Granite-related ore deposits. *Econ. Geol.* 350, 337–370.

Collins, W. J., Huang, H. Q., and Jiang, X. (2016). Water-fluxed crustal melting produces Cordilleran batholiths. *Geology* 44, 143–146. doi: 10.1130/g37398.1

Dejidmaa, G. (2003). *State Geological Complete Map*. Ulaanbaatar: Government of Mongolia. Report 5567.

DePaolo, D. J. (1988). *Neodymium Isotope Geochemistry: An Introduction*. New York, NY: Springer, 187.

Donskaya, T. V., Gladkochub, D. P., Mazukabzov, A. M., and Ivanov, A. V. (2013). Late Paleozoic - Mesozoic subduction-related magmatism at the southern margin of the Siberian continent and the 150 million-year history of the Mongol-Okhotsk Ocean. *J. Asian Earth Sci.* 62, 79–97. doi: 10.1016/j.jseaes.2012.07.023

Dorjsuren, B., and Bujinlkham, B. (2004). *State Geological Complete Map*. Ulaanbaatar: Government of Mongolia. Report 5668.

Dostal, J., and Chatterjee, A. K. (1995). Origin of topaz-bearing and related peraluminous granites of Late Devonian Davis Lake pluton, Nova Scotia, Canada: crystal versus fluid fractionation. *Chem. Geol.* 123, 67–88. doi: 10.1016/0009-2541(95)00047-p

Dostal, J., Owen, J. V., Gerel, O., Keppie, J. D., Corney, R., Shellnutt, J. G., et al. (2014). The 186 Ma Dashibalbar alkaline granitoid pluton in the North-Gobi rift of Central Mongolia: evidence for melting of Neoproterozoic basement above a plume. *Am. J. Sci.* 314, 613–648. doi: 10.2475/02.2014.06

Dostal, J., Kontak, D. J., Gerel, O., Shellnutt, J. G., and Fayek, M. (2015a). Cretaceous ongonites (topaz-bearing albite-rich microleucogranites) from Ongon Khairkhan, Central Mongolia: products of extereme magmatic fractionation and pervasive metasomatic fluid: rock interaction. *Lithos* 236-237, 173–189. doi: 10.1016/j.lithos.2015.08.003

Dostal, J., Owen, J. V., Shellnutt, J. G., Keppie, J. D., Gerel, O., and Corney, R. (2015b). Petrogenesis of the Triassic Bayan-Ulan alkaline granitic pluton in the North Gobi rift of central Mongolia: implications for the evolution of the Early Mesozoic granitoid magmatism in the Central Asian Orogenic Belt. *J. Asian Earth Sci.* 109, 50–62. doi: 10.1016/j.jseaes.2015.04.021

Eby, G. N. (1992). Chemical subdivision of the A-type granitoids: petrogenetic and tectonic implications. *Geology* 20, 641–644.

Förster, H. J., Tischendorf, G., Trumbull, R. B., and Gottesmann, B. (1999). Late-collisional granites in the Variscan Erzgebirge, Germany. *J. Petrol.* 40, 1613–1645. doi: 10.1093/petroj/40.11.1613

Frost, C. D., and Frost, B. R. (2011). On ferroan (A-type) granitoids: their compositional variability and mode of origin. *J. Petrol.* 52, 39–53. doi: 10.1093/petrology/egq070

Gao, S., Luo, T. C., Zhang, B. R., Zhang, H. F., Han, Y. W., Zhao, Z. D., et al. (1998). Chemical composition of the continental crust as revealed by studies in East China. *Geochim. Cosmochim. Acta* 62, 1959–1975. doi: 10.1016/s0016-7037(98)00121-5

Hanchar, J. M., and Watson, E. B. (2003). Zircon saturation thermometry. *Rev. Mineral. Geochem.* 53, 89–112. doi: 10.1515/9781501509322-007

Hartman, J., Franks, R., Gehrels, G., Hourigan, J., and Wenig, P. (2017). *Decoding Data Files from a Thermo ElementTM ICP Mass Spectrometer*. Available online at: https://github.com/jhh67/extractdat.git (accessed October 20, 2019).

Hoskin, P. W. O., and Schaltegger, U. (2003). The composition of zircon and igneous and metamorphic petrogenesis. *Rev. Mineral. Geochem.* 53, 27–62. doi: 10.1515/9781501509322-005

Huppert, H. E. and Sparks, R. S. J. (1988). The generation of granite magmas by intrusions of basalts into continental crust. *J. Petrol.* 29, 599–624. doi: 10.1093/petrology/29.3.599

Ivanova, G. F. (1976). *Mineralogy and Geochemistry of The Tungsten Deposits in Mongolia*. Moscow: Nauka.

Jackson, S. E., Pearson, N. J., Griffin, W. L., and Belousova, E. A. (2004). The application of laser ablation-inductively coupled plasma-mass spectrometry to in situ U–Pb zircon geochronology. *Chem. Geol.* 211, 47–69. doi: 10.1016/j.chemgeo.2004.06.017

Jahn, B. M., Litvinovsky, B. A., Zanvilevich, A. N., and Rechow, M. (2009). Peralkaline granitoid magmatism in the Mongolian-Transbaikalian Belt: evolution, petrogenesis and tectonic significance. *Lithos* 113, 521–539. doi: 10.1016/j.lithos.2009.06.015

Jahn, B.-M., Wu, F. Y., and Chen, B. (2000). Granitoids of the Central asian orogenic belt and continental growth in the phanerozoic. *Trans. R. Soc. Edinburgh Earth Sci.* 91, 181–193. doi: 10.1017/s0263593300007367

Jargalsaikhan, D. (1996). "Metallic mineral deposits," in *Guide to the Geology and Mineral resources of Mongolia*, eds D. Jargalsaikhan, M. Kazmer, and D. Sanjaadorj (Ulaanbaatar: MUST), 157–158.

Khasin, R. A. (1977). "Tin, tungsten and molybdenum," in *Geology of Mongolian People's Republic* (Moscow: Nedra), 270–436.

Korges, M., Weis, P., Lüders, V., and Laurent, O. (2017). Depressurization and boiling of a single magmatic fluid as a mechanism for tin-tungsten deposit formation. *Geology* 46, 75–78. doi: 10.1130/g39601.1

Kuzmin, M. I, Yarmolyuk, V. V., and Kravchinsky, V. A. (2010). Phanerozoic hot spot traces and paleogeographic reconstructions of the Siberian continent based on interaction with the African large low shear velocity province. *Earth Sci. Rev.* 102, 29–59. doi: 10.1016/j.earscirev.2010.06.004

Kylander-Clark, A. R. C., Hacker, B. R., and Cottle, J. M. (2013). Laser-ablation split-stream ICP petrochronology. *Chem. Geol.* 345, 99–112. doi: 10.1016/j.chemgeo.2013.02.019

Li, S., Wang, T., Wilde, S. A., and Tong, Y. (2013). Evolution, source and tectonic significance of Early Mesozoic granitoid magmatism in the Central Asian Orogenic Belt (central segment). *Earth Sci. Rev.* 126, 206–234. doi: 10.1016/j.earscirev.2013.06.001

Linnen, R. B. (1998). The solubility of Nb-Ta-Zr–Hf-W in granitic melts with Li and Li + F: constraints for mineralization in rare metal granites and pegmatites. *Econ. Geol.* 93, 1013–1025. doi: 10.2113/gsecongeo.93.7.1013

Linnen, R. L., and Cuney, M. (2005). "Granite-related rare-element deposits and experimental constraints on Ta-Nb-W-Sn-Zr-Hf mineralization," in *Rare-Element Geochemistry and Mineral Deposits*, eds R. L. Linnen and I. M. Samson (Newfoundland: Geological Association of Canada), 45–68.

Miller, C. F., McDowell, S. M., and Mapes, R. W. (2003). Hot and cold granites? Implications of zircon saturation temperatures and preservation of inheritance. *Geology* 31, 529–532.

Paton, C., Hellstrom, J., Paul, B., Woodhead, J., and Hergt, J. (2011). Iolite: freeware for the visualisation and processing of mass spectrometric data. *J. Anal. Atom. Spectr.* 26, 2508–2518.

Peccerillo, A., and Taylor, S. R. (1976). Geochemistry of Eocene calc-alkaline volcanic rocks from the Kastamonu area, Northern Turkey. *Contrib. Mineral. Petrol.* 58, 63–81. doi: 10.1007/BF00384745

Petrus, J. A., and Kamber, B. S. (2012). VizualAge: a novel approach to laser ablation ICP-MS U-Pb geochronology data reduction. *Geostand. Geoanal. Res.* 36, 247–270. doi: 10.1111/j.1751-908x.2012.00158.x

Pollock, J.C., Sylvester, P. J. and Barr, S. M. (2015). Lu-Hf zircon and Sm-Nd whole-rock isotope constraints on the extent of juvenile arc crust in Avalonia: examples from Newfoundland and Nova Scotia, Canada. *Can. J. Earth Sci.* 52, 161–181. doi: 10.1139/cjes-2014-0157

Romer, R. I., and Kroner, U. (2016). Phanerozoic tin and tungsten mineralization-tectonic control on the distribution of enriched protoliths and heat sources for crustal melting. *Gondwana Res.* 31, 60–95. doi: 10.1016/j.gr.2015.11.002

Salvi, S., and Williams-Jones, A. E. (2005). "Alkaline granite-syenite deposits," in *Rare-Element Geochemistry and Mineral Deposits*, eds R. L. Linnen and I. M. Samson (Newfoundland: Geological Association of Canada), 315–341.

Sengör, A. M. C., Natal'in, B. A., and Burtman, V. S. (1993). Evolution of Altaid tectonic collage and Paleozoic crustal growth in Eurasia. *Nature* 364, 299–307. doi: 10.1038/364299a0

Shaw, D. M. (1968). A review of K-Rb fractionation trends by covariation analysis. *Geochim. Cosmochim. Acta* 32, 573–601. doi: 10.1016/0016-7037(68)90050-1

Sillitoe, R. H., Halls, C., and Grant, J. N. (1975). Porphyry tin deposits in Bolivia. *Econ. Geol.* 70, 913–927. doi: 10.2113/gsecongeo.70.5.913

Sláma, J., Košler, J., Condon, D. J., Crowley, J. L., Gerdes A., Hanchar, J. M., et al. (2008). Plešovice zircon- new natural reference material for U-Pb and Hf isotopic microanalysis. *Chem. Geol.* 249, 1–35. doi: 10.1016/j.chemgeo.2007.11.005

Smirnov, V. N., Koval, P. V., Tsypulov Yu, P., Kovalenko, V. I, and Antipin, V. S. (1977). K-Ar age of granitoid associations in Khentei (Mongolia). *Dokl. Russ. Acad. Sci.* 232, 192–195.

Sun, S. S., and McDonough, W. F. (1989). "Chemical and isotopic systematics of oceanic basalts: implications for mantle composition and processes," in *Magmatism in the Ocean Basins*, eds A. D. Saunders and M. J. Norry (London: Geological Society London), 313–345. doi: 10.1144/gsl.sp.1989.042.01.19

Syritso, L. F., Badanina, E. V., Abusshkevich, V. S., Volkova, E. V., and Terekhov, A. V. (2018). Fertility of rare-metal peraluminous granites and formation conditions of tungsten deposits. *Geol. Ore Deposits* 60, 33–51. doi: 10.1134/s1075701518010063

Taylor, S. R., and McLennan, S. M. (1985). *The Continental Crust: Its Composition and Evolution*. Oxford: Blackwell Scientific, 312.

Thomas, R., Förster, H. J., Rickers, K., and Webster, J. D. (2005). Formation of extremely F-rich hydrous melt fractions and hydrothermal fluids during differentiation of highly evolved tin-granite magmas: a melt/fluid-inclusion study. *Contrib. Mineral. Petrol.* 148, 582–601. doi: 10.1007/s00410-004-0624-9

Watson, E. B., and Harrison, T. M. (1983). Zircon saturation revisited: temperature and composition effects in a variety of crustal magma types. *Earth Planet. Sci. Lett.* 64, 295–304. doi: 10.1016/0012-821x(83)90211-x

Webster, J., Thomas, R., Förster, H. J., Seltman, R., and Tappen, C. (2004). Geochemical evolution of halogen-enriched granite magmas and mineralizing fluids of the Zinwald tin-tungsten mining district, Erzgebirge, Germany. *Mineral. Deposita* 39, 452–472.

Whalen, J. B., Currie, K. L., and Chappell, B. W. (1987). A-type granites: geochemical characteristics, discrimination and petrogenesis. *Contrib. Mineral. Petrol.* 95, 407–419. doi: 10.1007/bf00402202

Wiedenbeck, M., Alle, P., Corfu, F., Griffin, W. L., Meier, M., Oberli, F., et al. (1995). Three natural zircon standards for U–Th–Pb, Lu–Hf, trace element and REE analyses. *Geostand. Newslett.* 19, 10–23.

Yarmolyuk, V. V., Kovalenko, V. I., Kozakov, I. K., Salnikova, E. B., Bibikova, E. V., Kovach, V. P., et al. (2008). The age of the Khangai batholith and the problem of batholith formation in Central Asia. *Doklady Earth Sci.* 423, 1223–1228. doi: 10.1134/s1028334x08080096

Yarmolyuk, V. V., Kovalenko, V. I., Salnikova, E. B., Budnikov, S. V., Kovach, V. P., Kotov, A. B., et al. (2002). Tectono-magmatic zoning, magma sources, and geodynamic of the Early Mesozoic Mongolo-Transbaikalian magmatic area. *Geotectonics* 36, 293–311.

Yarmolyuk, V. V., and Kuzmin, M. I. (2011). *Rifting and Silicic Large Igneous Provinces of the Late Paleozoic - Early Mesozoic in the Central Asia: Large Igneous Provinces Commission*. Available online at: http://www.largeigneousprovinces.org/11dec (accessed January 15, 2020).

Yarmolyuk, V. V., and Kuzmin, M. I. (2012). Late Paleozoic and Early Mesozoic rare-metal magmatism of Central Asia: stages, provinces, and formation settings. *Geol. Ore Deposits* 54, 313–333. doi: 10.1134/s1075701512050054

Yarmolyuk, V. V., Kuzmin, M. I., and Kozlovsky, A. M. (2013). Late Paleozoic-Early Mesozoic within-plate magmatism in North Asia: traps, rifts, giant batholiths, and the geodynamics of their origin. *Petrology* 21, 101–126. doi: 10.1134/s0869591113010062

Conflict of Interest: The authors declare that the research was conducted in the absence of any commercial or financial relationships that could be construed as a potential conflict of interest.

The handling editor declared a past co-authorship with one of the authors, JD.

Copyright © 2020 Dostal, Svojtka, Gerel and Corney. This is an open-access article distributed under the terms of the Creative Commons Attribution License (CC BY). The use, distribution or reproduction in other forums is permitted, provided the original author(s) and the copyright owner(s) are credited and that the original publication in this journal is cited, in accordance with accepted academic practice. No use, distribution or reproduction is permitted which does not comply with these terms.